



# Study of Growing Ni Nanoparticles Loaded on Layered Inorganic-Imidazoline Covalently Bonded Hybrids Under a Transmission Electron Microscope

Kazuko Fujii<sup>1</sup> · Keiji Kurashima<sup>1</sup> · Hideo Hashizume<sup>1</sup> · Shuichi Shimomura<sup>1</sup> · Takatsugu Wakahara<sup>1</sup> · Toshihiro Ando<sup>1</sup>

Received: 26 July 2020 / Accepted: 9 September 2020 / Published online: 19 September 2020  
© Springer Science+Business Media, LLC, part of Springer Nature 2020

## Abstract

This study investigates nanoclusters loaded on layered inorganic-imidazoline covalently bonded hybrids. To reveal the existence of nanoclusters, transmission electron microscopy (TEM) and selected-area diffraction (SAD) analyses were performed. An imidazolyl group bonded covalently with an inorganic layer, which contained Ni<sup>2+</sup> (and not Mg<sup>2+</sup>) as an octahedral cation, in the layered hybrids. In this study, the layered hybrids synthesized at 170 and 150 °C are referred to as Ni-Im<sub>170</sub> and Ni-Im<sub>150</sub>, respectively. The TEM observations confirmed the presence of nanoclusters of 1–2 nm in diameter on thin sheets of Ni-Im<sub>170</sub> and Ni-Im<sub>150</sub>. The nanoclusters appeared as dark dots in the bright-field images and were brighter than the thin sheets in dark-field images. The SAD analyses exhibited halo patterns similar to those of phyllosilicates at the beginning of the TEM observations. The TEM analyses further revealed that the nanoclusters in both Ni-Im<sub>170</sub> and Ni-Im<sub>150</sub> grew into Ni nanoparticles (3–5 nm diameter) under TEM. The SAD analyses demonstrated diffraction patterns with a weak ring with a *d*-value of 0.20 nm and/or diffraction patterns attributed to Ni exhibiting rings with *d*-values of 0.20, 0.18, 0.12, and 0.11 nm after the nanocluster growth. Furthermore, in the case of Ni-Im<sub>150</sub>, drastic growth was observed under TEM, i.e., the diameters increased to approximately 30 nm.

**Keywords** Layered inorganic–organic hybrid · Nanocluster · Ni nanoparticle · Phyllosilicate

## 1 Introduction

Layered inorganic/organic complexes have been extensively investigated as potential candidates for novel solid-state materials with various functionalities and properties (optical, electrical, magnetic properties, etc.). Many layered inorganic/organic complexes have been prepared by intercalating organic species into the interlayer spaces of inorganic materials, such as 2:1 phyllosilicates and layered double hydroxides. The synthesis of layered inorganic–organic hybrids consisting of inorganic layers covalently bonded with

organic groups has been reported using one-pot synthesis [1–15] and post-grafting [16, 17]. In the present study, such hybrids have been referred to as ‘layered inorganic–organic covalently bonded hybrids’.

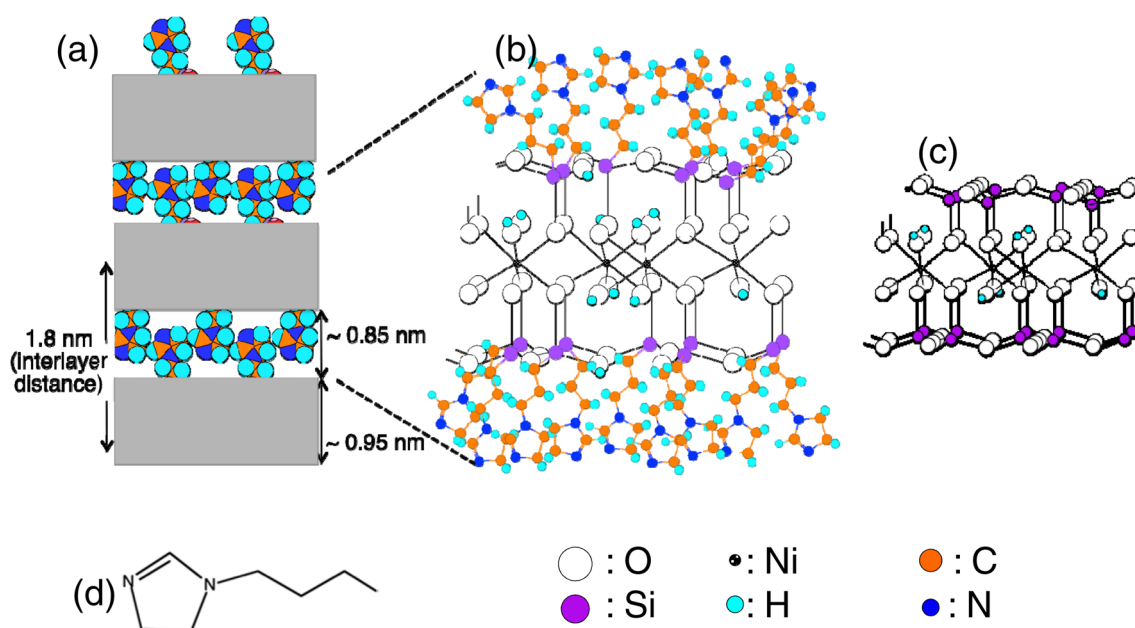
We have previously reported the synthesis of layered inorganic-imidazoline covalently bonded hybrids [18]. In a few studies, Ni<sup>2+</sup> has been considered as an octahedral cation for the inorganic layer of such hybrids. Scheme 1 represents the proposed model of the hybrids with Ni<sup>2+</sup> based on analytical results [18]. In the proposed model, an imidazolyl group is located within the interlayer space and bonds to the inorganic layer via a covalent bond.

The X-ray diffraction (XRD) measurements revealed XRD peaks assigned to nickel (Ni) in the case of the hybrid (Ni-Im<sub>170</sub>) synthesized at 170 °C; however, such peaks were not observed for the other hybrid (Ni-Im<sub>150</sub>) synthesized at 150 °C. Elemental analyses revealed a significant amount of Ni present in the layered inorganic-imidazoline covalently bonded hybrids. These results suggest the existence of Ni nanoclusters in Ni-Im<sub>150</sub>, indicating the

**Electronic supplementary material** The online version of this article (<https://doi.org/10.1007/s10904-020-01753-w>) contains supplementary material, which is available to authorized users.

✉ Kazuko Fujii  
FUJII.Kazuko@nims.go.jp

<sup>1</sup> National Institute for Materials Science (NIMS), 1-1 Namiki, Tsukuba, Ibaraki 305-0044, Japan



**Scheme 1** Schematic representation of **a** and **b** models proposed in the previous report [18], **a** the layered inorganic-imidazoline covalently bonded hybrids and **b** a layer of the hybrids, **c** 2: 1 layer of

smectite, and **d** imidazolyl group. The schemes **a** and **b** are modified form of Scheme 2 of the previous report [18]

possibility of directly synthesized layered hybrids loaded with Ni nanoclusters.

Ni nanoparticles, including nanoclusters, act as magnetic materials, sensors, conductive paste [19], internal electrodes [20], junction materials [21], adsorbents with high spillover activity for hydrogen [22], catalysts for hydrogenation of aromatics [23], and H<sub>2</sub> production [24]. Recently, extensive studies have been reported on the synthesis of Ni nanoparticles using various methods, including chemical reduction in aqueous solutions [25, 26] and chemical vapour deposition [21]. However, many of these synthesized Ni nanoparticles were larger than 100 nm and tended to agglomerate among themselves. It is important to control the particle sizes and prevent the agglomeration of metals for improved activities. Hence, novel techniques have been investigated to prepare fine Ni nanoparticles using solid supports, such as zeolites [23, 27–31], carbon templates [22, 32, 33], and Al<sub>2</sub>O<sub>3</sub> [24]. Interestingly, a few investigations have successfully achieved the synthesis of fine Ni nanoparticles and nanoclusters smaller than 5 nm [22, 27, 28, 30, 31, 34, 35]. Nishihara et al. [22] reported a high hydrogen chemisorption ability and high hydrogen spillover activity comparable to those of Pt nanoparticles for synthesized Ni nanoclusters loaded on zeolite-templated carbon (ZTC).

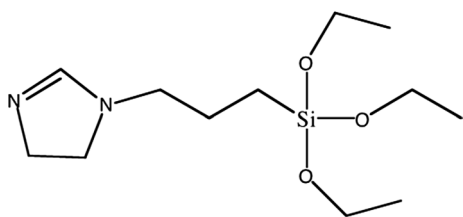
Recent studies have investigated the synthesis of Cu, Au, and Ag nanoparticles by adding layered clay minerals, i.e., phyllosilicates [36, 37] and phyllosilicate/organic complexes [38, 39], as solid supports.

The aim of the present study is to reveal the existence of nanoclusters in Ni-Im<sub>170</sub> and Ni-Im<sub>150</sub> hybrids, indicating the successful direct synthesis of layered inorganic-imidazoline covalently bonded hybrids loaded with nanoclusters. The transmission electron microscopy (TEM) images (both bright- and dark-field) and SAD analyses revealed nanoclusters with diameters of 1–2 nm loaded on thin sheets of Ni-Im<sub>170</sub> and Ni-Im<sub>150</sub>. Furthermore, for both Ni-Im<sub>170</sub> and Ni-Im<sub>150</sub>, the nanoclusters grew to the size of Ni nanoparticles with diameters of 3–5 nm under TEM. The TEM analyses revealed a drastic growth of the nanoclusters to Ni nanoparticles with a diameter of approximately 30 nm in Ni-Im<sub>150</sub>. The present study has proposed a new method to synthesize nanoclusters and control the sizes of nanoclusters and nanoparticles.

## 2 Experimental

### 2.1 Synthesis and Characterisation of the Layered Inorganic-Imidazoline Covalently Bonded Hybrids

Layered inorganic-imidazoline covalently bonded hybrids were synthesized as per a previously reported study [18]. Nickel (II) acetate tetrahydrate (Ni(CH<sub>3</sub>COO)<sub>2</sub>·4H<sub>2</sub>O) and triethoxy-3-(2-imidazolin-1-yl)propylsilane (C<sub>12</sub>H<sub>26</sub>N<sub>2</sub>O<sub>3</sub>Si, abbreviated as ITES [5], Scheme 2) were used in two separate reactions, corresponding to temperatures of 170 and



**Scheme 2** Triethoxy-3-(2-imidazolyl)propylsilane (ITES)

150 °C for 6 days each (see Electronic Supplementary Material). The crude products after the reaction were washed with purified water several times and then freeze-dried. The synthesis methods are described in detail elsewhere [18]. In this study, the samples separately synthesized at 170 and 150 °C are denoted as Ni-Im<sub>170</sub> and Ni-Im<sub>150</sub>, respectively.

Ni-Im<sub>170</sub> and Ni-Im<sub>150</sub> were characterised by inductively coupled plasma optical emission spectrometry (ICP-OES), CHN analysis, thermogravimetric and differential thermal analysis (TG–DTA), XRD, scanning electron microscopy (SEM), Fourier transform infrared (FT-IR) spectroscopy, ultraviolet–visible–near-infrared (UV–VIS–NIR) spectroscopy, and fluorescence spectrophotometry, which are described in detail elsewhere [18].

## 2.2 TEM Observation

The microstructures of Ni-Im<sub>170</sub> and Ni-Im<sub>150</sub> were examined using a TEM (JEOL JEM1010), under the settings of 100 kV accelerating voltage and 2–120 pA/cm<sup>2</sup> illumination beam current. We observed both bright- and dark-field images and selected-area diffraction (SAD) patterns. To prepare the specimens for the TEM observations, each powder sample of Ni-Im<sub>170</sub> and Ni-Im<sub>150</sub> was dispersed in acetone ((CH<sub>3</sub>)<sub>2</sub>CO), and a few microliters of each mixture was dropped on the microgrid using a micropipette. All the specimens were air-dried before the TEM observations.

## 3 Results and Discussion

### 3.1 Structure and Composition of the Layered Inorganic-Imidazoline Covalently Bonded Hybrids (Ni-Im<sub>170</sub> and Ni-Im<sub>150</sub>)

The analytical results have led us to the proposed model of Ni-Im<sub>150</sub> as shown in Scheme 1. We have already reported the analytical results along with the proposed model and composition details elsewhere [18], excluding the composition and structure of Ni-Im<sub>170</sub>. In this section, we briefly summarise the proposed models and compositions of Ni-Im<sub>170</sub> and Ni-Im<sub>150</sub> which are necessary for understanding the results and discussion in the following sections.

The proposed model is a layered structure comprising inorganic layers with an imidazolyl group located between them, wherein the interlayer distances for Ni-Im<sub>170</sub> and Ni-Im<sub>150</sub> are 1.9 nm and 1.8 nm, respectively. The inorganic layer and imidazolyl group bond covalently with each other via a Si–C covalent bond. The inorganic layer refers to the 2:1 phyllosilicate-like layer formed by a cationic octahedral sheet sandwiched between the two siloxane sheets, wherein the octahedral cation is Ni<sup>2+</sup>.

The 2:1 phyllosilicates have layered structures with each layer consisting of a cation (such as Mg<sup>2+</sup> and Al<sup>3+</sup>) sheet sandwiched between the two-dimensional Si tetrahedral sheets. Each SiO<sub>4</sub> tetrahedron shares three corners with the neighbouring tetrahedra to form links and construct the tetrahedral Si sheets with a hexagonal mesh pattern. Divalent octahedral cations, such as Mg<sup>2+</sup>, occupy all the cation sites of the octahedral sheet in the ideal structures of 2:1 trioctahedral phyllosilicates. The layers exhibit negative charge in many groups of phyllosilicates (e.g., smectite) due to diadochy isomorphous substitutions. To compensate for the negative charge, exchangeable cations are intercalated between the layers of phyllosilicates. Typical trioctahedral smectites are hectorite (M<sub>x</sub>(Mg<sub>3-x</sub>Li<sub>x</sub>)Si<sub>4</sub>O<sub>10</sub>(OH)<sub>2</sub>), stevensite (M<sub>2x</sub>(Mg<sub>3-x</sub>)Si<sub>4</sub>O<sub>10</sub>(OH)<sub>2</sub>), and saponite (M<sub>y-x</sub>(Mg<sub>3-x</sub>(Al, Fe)<sub>x</sub>)Si<sub>4-y</sub>Al<sub>y</sub>O<sub>10</sub>(OH)<sub>2</sub>), where M is the monovalent exchangeable cation between the layers. These compositions are written for the case of monovalent exchangeable cations (M). There are vacancies in the octahedral sheet of stevensite.

The ionic radius of Ni<sup>2+</sup> is 0.069 nm. The ionic radius of Mg<sup>2+</sup> is 0.072 nm [40, 41]. A six-coordinated octahedron is formed with Ni as the central metal. Therefore, we adopted Ni<sup>2+</sup> to synthesize layered inorganic-imidazoline hybrids, wherein Ni<sup>2+</sup> is not available as the main element for the octahedral cation in the natural phyllosilicates.

The XRD pattern of Ni-Im<sub>170</sub> exhibited the reflection peaks attributed to nickel metal crystals ( $d=0.204$  and 0.176 nm) in addition to the peaks ascribed to the phyllosilicate-like layer (1.9, 0.95, 0.46, 0.26, and 0.155 nm) [18] (see Electronic Supplementary Material). However, no XRD peaks attributed to nickel metal crystals were observed in the XRD pattern of Ni-Im<sub>150</sub>. Furthermore, the XRD pattern of Ni-Im<sub>150</sub> confirmed the peaks ascribed to the phyllosilicate-like layer, whereas no peaks were attributed to the starting reagents and by-products such as nickel oxide. The analytical results (from XRD, FT-IR, etc.) revealed that Ni-Im<sub>170</sub> is a mixture of the layered inorganic-imidazoline covalently bonded hybrids and Ni metal crystals.

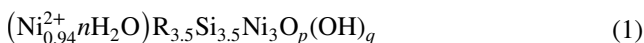
Table 1 lists the mole ratios calculated based on the elemental contents obtained by the ICP-OES and CHN analyses. The molar ratios are given as 3.5:9.1:20.7:63.0:5.4 for Si:Ni:C:H:N corresponding to Ni-Im<sub>150</sub> and 3.5:7.7:16.8:52.7:4.2 for Si:Ni:C:H:N corresponding to

**Table 1** Mole ratios calculated from the results of elemental analyses

|                      | Si   | Ni   | C     | H     | N    | C/Si | Ni/Si |
|----------------------|------|------|-------|-------|------|------|-------|
| Ni-Im <sub>150</sub> | 3.50 | 9.11 | 20.66 | 63.02 | 5.36 | 5.9  | 2.6   |
| Ni-Im <sub>170</sub> | 3.50 | 7.73 | 16.81 | 52.67 | 4.15 | 4.8  | 2.2   |

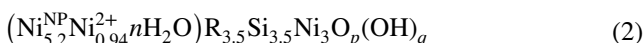
Ni-Im<sub>170</sub>. The weight contents are listed in the Electronic Supplementary Material (Table S1). Additionally, oxygen was obtained as a residue.

Considering the proposed model (Scheme 1) and composition reported for a layered inorganic-imidazoline covalently bonded hybrid with Mg<sup>2+</sup> as the octahedral cation [18], a tentative composition can be given as follows:

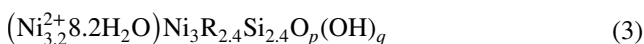


where R denotes the imidazolyl group, (2-imidazolin-1-yl)propyl group (C<sub>6</sub>H<sub>11</sub>N<sub>2</sub>).

The Ni/Si molar ratio is 1.13 in chemical formula (1). In contrast, the elemental analyses indicated large Ni/Si molar ratios of 2.2 in Ni-Im<sub>170</sub> and 2.6 in Ni-Im<sub>150</sub>. The molar ratios of excess Ni to Si were 1.1 and 1.5 for Ni-Im<sub>170</sub> and Ni-Im<sub>150</sub>, respectively. The large molar ratio of Ni/Si was apparently reasonable at this stage for Ni-Im<sub>170</sub>, as the XRD measurement confirmed the presence of Ni metal crystals in Ni-Im<sub>170</sub>. Interestingly, the excess amount of Ni suggested the presence of Ni nanoclusters in Ni-Im<sub>150</sub>. Based on these analytical results and discussion, the composition calculated for Ni-Im<sub>150</sub> can be given as follows:



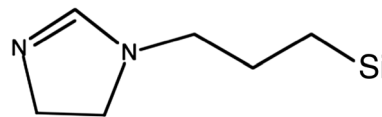
where Ni<sup>NP</sup> is a single Ni atom in Ni nanoclusters. Although the samples were washed with H<sub>2</sub>O several times before the analyses, the excess Ni within the interlayer space was not removed by H<sub>2</sub>O. Another tentative composition of Ni-Im<sub>150</sub>, without considering Ni nanoclusters, can be given as follows:



Each Si atom would be located far from its nearest neighbouring Si atom with chemical formula (3), as illustrated in Scheme S1 (see Electronic Supplementary Material), indicating hardly any Si–O–Si network formation in the model (Scheme S1).

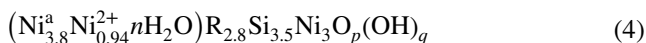
The RSiO<sub>3</sub> units can be linked for the formation of a continuous two-dimensional organosiloxane (Scheme 1) with chemical formula (2), whereas the hexagonal mesh pattern of the Si tetrahedron is not formed, as discussed in detail in a previous report [18].

Table S1 lists the elemental contents (in weight percent) of Ni-Im<sub>150</sub> and Ni-Im<sub>170</sub> (see Electronic Supplementary Material). Notably, a higher Si content was found in

**Scheme 3** Imidazolylsilyl group

Ni-Im<sub>170</sub> than in Ni-Im<sub>150</sub>. The higher Si content suggests the coexistence of amorphous Si in the Ni-Im<sub>170</sub> specimen. The molar ratios of C/Si in Ni-Im<sub>170</sub> and Ni-Im<sub>150</sub> are 4.8 and 5.9, respectively, whereas such molar ratio is 6 for the imidazolylsilyl group, 3-(2-imidazolin-1-yl)propylsilyl group (C<sub>6</sub>H<sub>11</sub>N<sub>2</sub>Si, Scheme 3). These analytical results indicate the possibility of a part of the imidazolylsilyl group being decomposed during the synthesis procedure at 170 °C. It is well known that the background around the *d*-value of 0.4 nm (around 2θ of 20° with CuKα) is observed in the XRD patterns of samples, including the amorphous phases consisting mainly of Si, O, and H. However, the background was not large in the XRD pattern of Ni-Im<sub>170</sub> in comparison with that of Ni-Im<sub>150</sub> (see Electronic Supplementary Material). An amorphous morphology was not observed for both Ni-Im<sub>170</sub> and Ni-Im<sub>150</sub> under TEM in this study. These experimental results indicated that the amount of amorphous phase would not be much higher in Ni-Im<sub>170</sub> than in Ni-Im<sub>150</sub>.

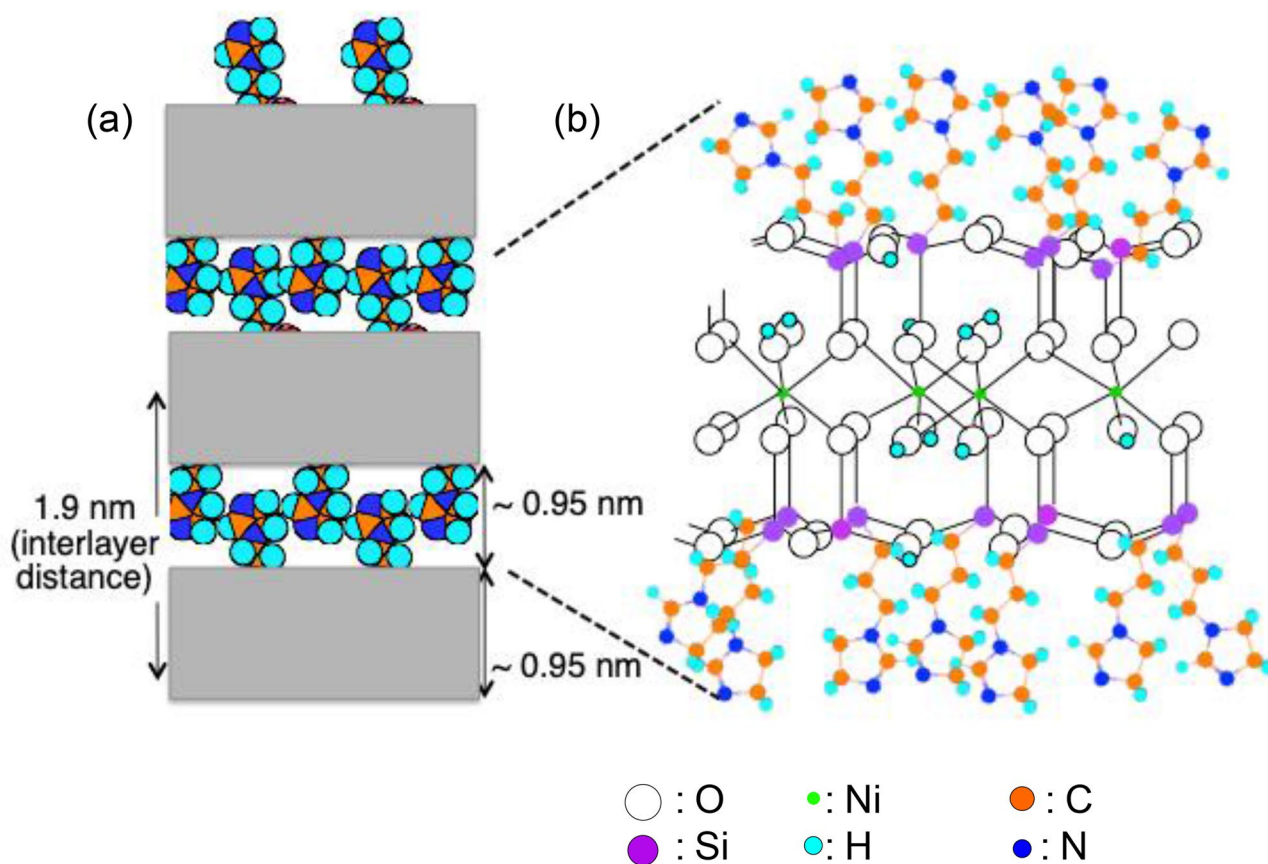
With the assumption of the partial decomposition of the imidazolylsilyl group and the analytical results, the composition of Ni-Im<sub>170</sub> can be calculated as follows:



where Ni<sup>a</sup> corresponds to the total sum of excess Ni atoms in the Ni nanoclusters and bulk Ni metal crystal. In the structure of formula (4), a part of Si bonds with three oxygen atoms and forms a covalent bond with one imidazolyl group, whereas the other part of Si bonds with four oxygen atoms (Scheme 4). However, all Si atoms bond covalently with the imidazolyl group in the model structure of Ni-Im<sub>150</sub> (Scheme 1).

### 3.2 TEM Images for Ni-Im<sub>170</sub> and Ni-Im<sub>150</sub>

Figure 1a shows a TEM image of Ni-Im<sub>170</sub>, comprising thin sheets that overlapped with each other. A stacked morphology denoted by an arrow was observed on the edge from a direction nearly parallel to the stacking direction of the



**Scheme 4** Schematic of proposed models for  $\alpha$  Ni-Im<sub>170</sub> and **b** a layer of Ni-Im<sub>170</sub>

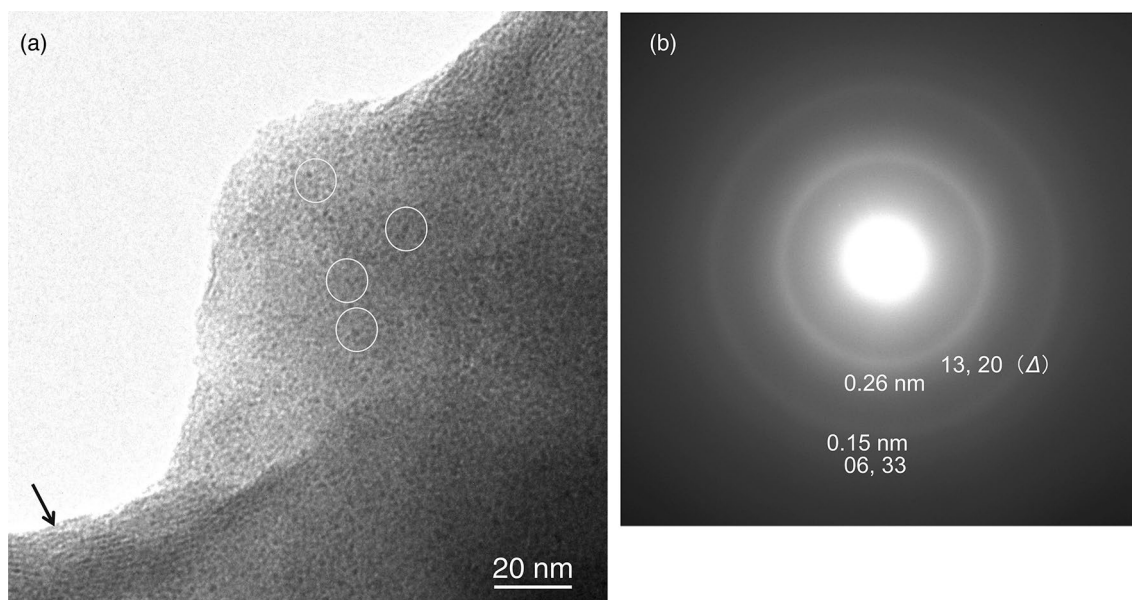


**Fig. 1** **a** Transmission electron microscopy (TEM) image and **b** selected-area diffraction (SAD) pattern for Ni-Im<sub>170</sub>

thin sheets. Numerous nanoclusters with small diameters (1 nm) and without any aggregation were observed on the thin sheets. We marked some of the nanoclusters with circles as guides in Fig. 1a. In this study, particles smaller than 3 nm are referred to as nanoclusters.

It is difficult to observe sub-nanoclusters (particles smaller than 1 nm) under TEM owing to their small size and poor structures, even if sub-nanoclusters are present in the specimen. A sub-nanocluster, assumed as a sphere with a diameter of 0.5 nm, can barely accommodate 48 Ni atoms (with a  $\text{Ni}^{2+}$  ion radius of 0.069 nm [40, 41]) and thus hardly form an assembly ordered enough to produce TEM images. In contrast, 380 Ni atoms can exist in a sphere with a diameter of 1 nm, and 3044 Ni atoms can exist in a sphere with a diameter of 2 nm.

The nanoclusters appeared as dark dots (Fig. 1a). Heavy atoms produce images with high contrast in TEM observations, similar to objects with high densities.

The diameters were larger than 5 nm for most reported Ni nanoparticles loaded on the templates, e.g., zeolites [22, 24, 32, 33]. A few studies have successfully achieved the synthesis of Ni nanoparticles with diameters of less than 5 nm (2–5 nm) loaded on zeolites [27, 28, 30, 31]. A study based on the synthesis of Cu nanoparticles in aqueous media with dispersed synthetic saponite reported nanoparticles with diameters of 6–24 nm [36, 37]. Saponite is one of the 2:1 trioctahedral phyllosilicates. Thus the diameters of the nanoclusters in Ni-Im<sub>170</sub> were smaller (approximately 1 nm) than those of the reported metal nanoparticles.

As shown in Fig. 1b, the electron diffraction pattern exhibits a halo pattern similar to those of 2:1 trioctahedral

phyllosilicates, with *d*-values of 0.26 and 0.15 nm corresponding to the inner and outer rings, respectively. The electron diffraction data were assigned to the 13, 20 (around 0.26 nm) and 06, 33 (around 0.15 nm) bands for 2:1 trioctahedral phyllosilicates, e.g., hectorite and stevensite.

The TEM images of other areas on the Ni-Im<sub>170</sub> specimen showed numerous nanoclusters with small diameters without any aggregations or bulk morphology attributed to bulk Ni metal crystals, similar to the area in Fig. 1a. Furthermore, the SAD analyses revealed patterns for the other areas similar to those of 2:1 trioctahedral phyllosilicates.

Although the XRD pattern exhibited XRD peaks attributed to Ni metal crystals (see Fig. S1 in the Electronic Supplementary Material), the TEM image and SAD diffraction pattern attributed to Ni metal crystals was not observed. For Ni metal crystals, the density is higher and the aspect ratio is lower in comparison with those of the layered hybrid loaded with nanoclusters. The bulk Ni metal crystal becomes settled in the liquid mixture of Ni-Im<sub>170</sub> and acetone during the TEM specimen preparation. The nanoclusters loaded on the layered inorganic-imidazoline covalently bonded hybrid would be placed on the TEM grid. A discussion on the SAD pattern details is presented in the next section.

The TEM image of Ni-Im<sub>150</sub> in Fig. 2a shows thin sheets overlapped with a few other thin sheets. Nanoclusters with significantly small diameters (1 nm) were found on the thin sheets of Ni-Im<sub>150</sub>, similar to that of Ni-Im<sub>170</sub>. However, there were less nanoclusters observed on Ni-Im<sub>150</sub> than on Ni-Im<sub>170</sub>. Interestingly, the excess amounts of Ni determined by the elemental analyses of Ni-Im<sub>150</sub> suggested the presence of sub-nanoclusters

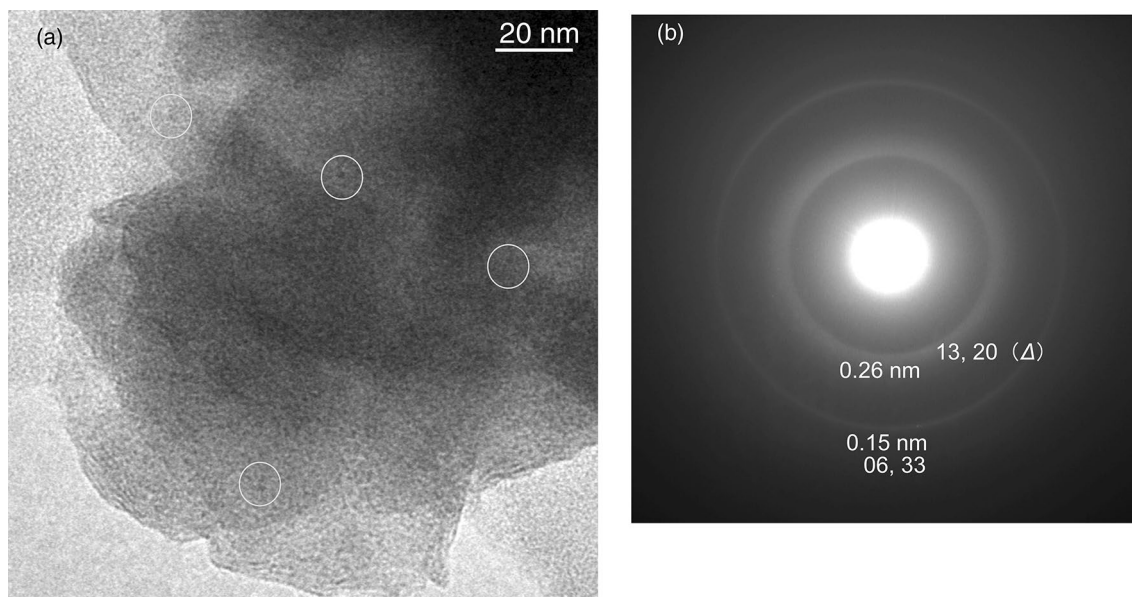


**Fig. 2** a TEM image and b SAD pattern for Ni-Im<sub>150</sub>

smaller than 1 nm. Thus, only a fraction of the excess Ni was observed owing to the small number of atoms and low crystallinity of the sub-nanoclusters, as previously described.

The electron diffraction pattern of Ni-Im<sub>150</sub> showed a halo pattern similar to those of 2:1 trioctahedral phyllosilicates, as shown in Fig. 2b, with *d*-values of 0.26 and 0.15 nm corresponding to the diffraction rings. The inner ring (*d* = 0.26 nm) is bright at the inside edge and becomes gradually dimmer towards the outer side of the diffraction ring. This phenomenon is consistent with the results of the XRD measurement, which exhibits delta diffraction peaks for phyllosilicates, Ni-Im<sub>170</sub>, and Ni-Im<sub>150</sub> (see Electronic Supplementary Material).

In this study, we proposed a method for the synthesis of nanoclusters with a small diameter (approximately 1 nm). Initially, ITES was slowly added to the aqueous solution of Ni acetate to synthesize Ni-Im<sub>170</sub> and Ni-Im<sub>150</sub>, with subsequent stirring at room temperature (RT). It is well known that imidazolines coordinate to heavy metals. The imidazolyl group of ITES would coordinate to a part of Ni<sup>2+</sup> in the mixtures under stirring. The other part of Ni<sup>2+</sup> needs to be incorporated into the octahedral sheet of the phyllosilicate-like layer upon reacting with a silanol group of hydrolysed ITES, an alkoxy-silyl group of ITES, and H<sub>2</sub>O. These reactions should proceed under stirring at RT and subsequent heat treatments at 170 °C or 150 °C for the respective hybrid. The imidazolyl group remained within the interlayer space of the Ni-Im<sub>170</sub> and Ni-Im<sub>150</sub> hybrids by maintaining the coordination to Ni<sup>2+</sup>. A part of the coordinated Ni<sup>2+</sup> within the interlayer space would compensate for the negative charge of the layer. The other part of Ni<sup>2+</sup> forms the Ni nanoclusters (1 nm in diameter) within the interlayer space (confined two-dimensional nano-space).

### 3.3 Growth of the Nanoclusters Under TEM

A series of TEM images was analysed for the changes. Various settings with respect to the objective aperture (see Electronic Supplementary Material) were used in this study to observe the bright-field and dark-field images, which are especially important for objectives with the heavy atoms producing bright images in dark-field images. Indeed, dark-field images are generally analysed to study lattice defects, such as dislocations.

The bright-field image of Ni-Im<sub>150</sub> in Fig. 3a shows aggregated thin sheets and only a small amount of nanoclusters with a diameter of 1 nm. The dark-field image (Fig. 3b), following the bright-field image (Fig. 3a), was studied to analyse the microstructure of Ni-Im<sub>150</sub> with different contrasts.

The second dark-field image (Fig. 3c), taken approximately 5 min after the first dark-field image (Fig. 3b), revealed that the nanoclusters grew into larger nanoparticles of 3 nm in diameter (with 5 min having elapsed due to focus adjustments after Fig. 3b was taken). These changes in the TEM images suggest that the nanoclusters grown under TEM were due to the irradiation of the electron beam.

To demonstrate the changes in the microstructures of Ni-Im<sub>150</sub> under TEM, bright- and dark-field images were analysed (Fig. 4). The bright-field image (Fig. 4a) showed a few nanoclusters (2 nm in diameter) on the thin sheets. The TEM image taken after 1 min revealed that the nanoclusters grew to nanoparticles (3 nm in diameter) in addition to the presence of numerous nanoparticles (Fig. 4b). The corresponding SAD pattern was analysed (Fig. 4c) after the TEM analysis; this pattern showed a weak ring with a *d*-value of 0.20 nm. Although the *d*-value for the 111 plane of Ni is 0.2034 nm [42], it would be hasty to assign indices for such a diffraction pattern exhibiting only one broad ring.

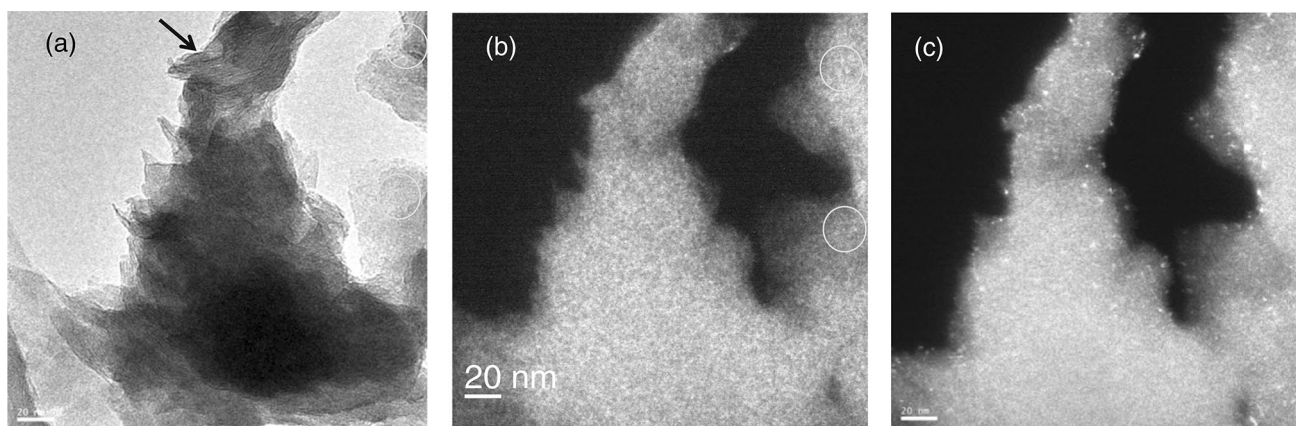


**Fig. 3** a Bright-field image and b and c dark-field images for Ni-Im<sub>150</sub>

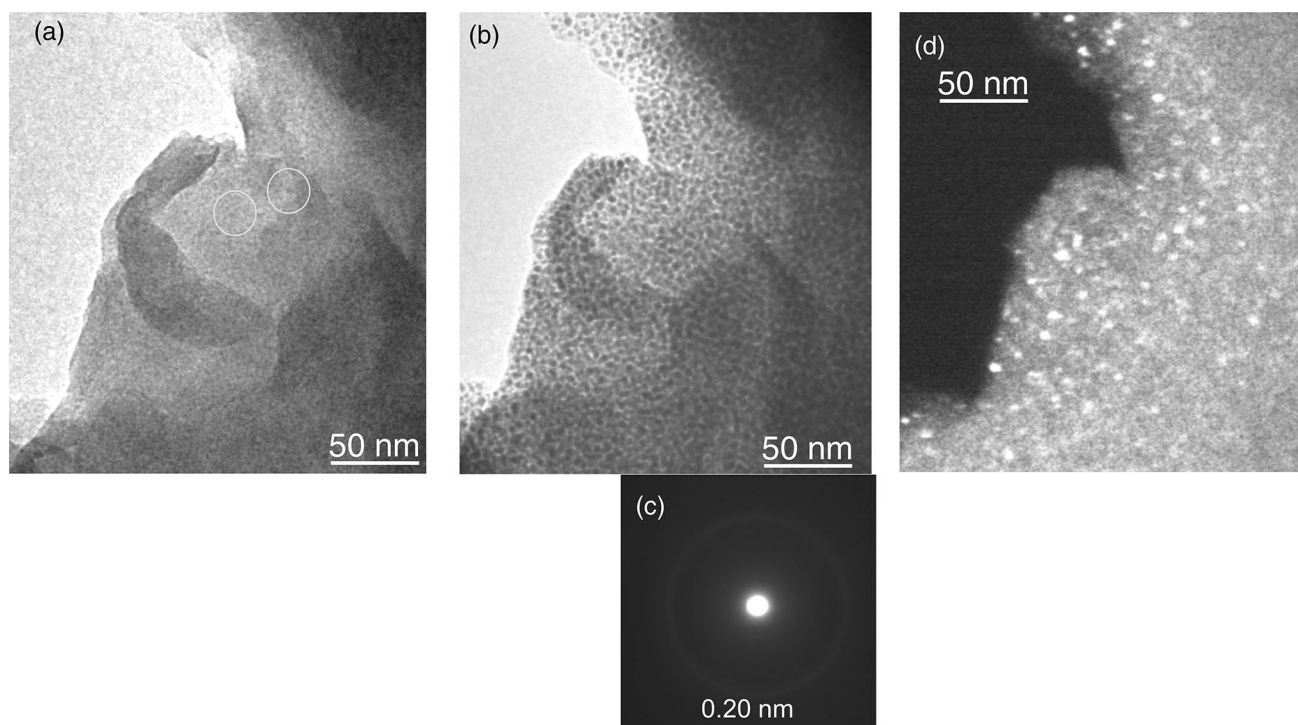


**Fig. 4** **a** and **b** Bright-field images, **d** dark-field image, and **c** SAD pattern for Ni-Im<sub>150</sub>

Furthermore, the dark-field image (Fig. 4d) examined under TEM indicated that the nanoparticles further grew to sizes of 3–5 nm and were brighter than the thin sheets visible in the same image. This result suggests that the nanoparticles in Fig. 4b and d are Ni nanoparticles, as Ni is the heaviest atom in Ni-Im<sub>150</sub> (heavy atoms exhibit bright features in dark-field images). There were less bright spots in the dark-field image (Fig. 4d) than the dark spots in the bright-field image (Fig. 4b). The SAD pattern (Fig. 4c) showed a diffraction ring, which is produced for crystals with disordered orientations. The dark-field image (Fig. 4d) exhibited bright spots corresponding to Ni nanoparticles with the crystal orientation matching with a part of the objective aperture set.

The SAD pattern of Ni-Im<sub>150</sub> (Fig. 4c) exhibiting only one broad and weak ring indicates that the crystallinity of the nanoparticles would be low and the amount of nanoparticles would not be sufficient to produce diffraction rings of stronger intensity, even after the TEM observations. The (111) diffraction is the strongest among the diffractions of a Ni metal crystal [42]. The other diffractions of a Ni metal crystal would be too weak to appear in the SAD pattern (Fig. 4c) of Ni-Im<sub>150</sub> even after the TEM observation.

The SAD pattern did not show any diffraction rings attributed to the 2:1 phyllosilicate-like structure (Fig. 4c). The results (Fig. 4b, c) indicated a broken phyllosilicate-like structure with the remaining morphology of the thin sheets during the TEM observation. This breakage could be

the reason for recognition of significantly weak diffraction ring in the SAD pattern (Fig. 4c). In contrast, the SAD patterns of Ni-Im<sub>170</sub> and Ni-Im<sub>150</sub> at the beginning of the TEM observations did not exhibit any diffraction rings or spots corresponding to Ni metal crystals (Figs. 1b, 2b). However, they exhibited broad diffraction rings attributed to the 2:1 phyllosilicate-like layer. We hardly recognised the very weak rings because of the background due to the 2:1 phyllosilicate-like layer, even if the SAD analysis may have produced a very weak ring similar to that in Fig. 4c. Considering the description of the above SAD patterns, another interpretation suggests that the SAD patterns (Figs. 1b, 2b) would indicate amorphous nanoclusters.

It is important to note that we cannot observe the microstructure under TEM before the irradiation from the electron beam, even at the first observation.

A series of images was studied to observe changes in the microstructure of Ni-Im<sub>170</sub> under TEM (Fig. 5). The nanoclusters of 2 nm in diameter were seen on the thin sheets at the first observation, as shown in the bright-field image (Fig. 5a). The SAD pattern exhibited broad rings with *d*-values of 0.26 and 0.15 nm (Fig. 5b), similar to those of 2:1 trioctahedral phyllosilicates. Several observations were carried out in series involving a bright-field observation (Fig. 5c), SAD analysis (Fig. 5d), and a dark-field observation (Fig. 5e). The nanoclusters grew slightly from 2 nm (Fig. 5a) to 3 nm in size (Fig. 5c, e). The SAD



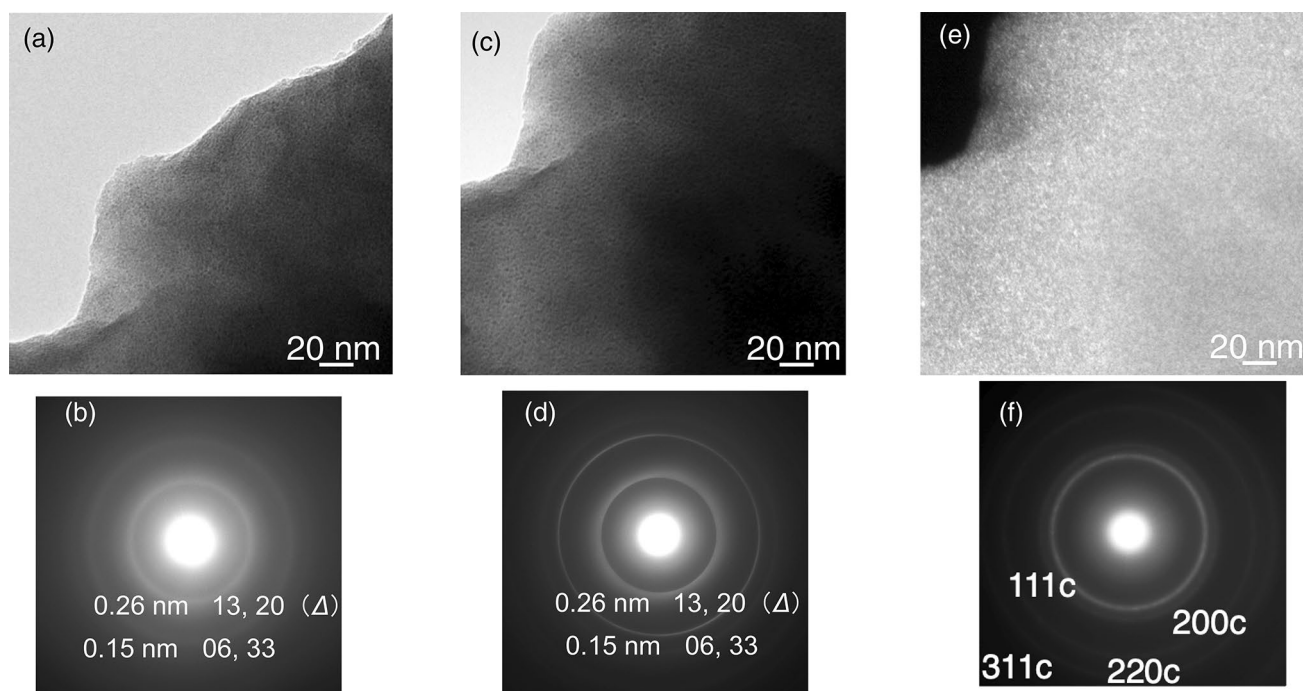


**Fig. 5** a and c Bright-field images, e dark-field image, and b, d and f SAD patterns for Ni-Im<sub>170</sub>

analysis showed halo pattern (Fig. 5d) similar to those of 2:1 trioctahedral phyllosilicates. Then we observed the dark-field image (Fig. 5e). Next, SAD analysis was performed, demonstrating a diffraction pattern attributed to Ni (Fig. 5f). Several *d*-values of 0.20 (the strongest and innermost ring), 0.18 (a weak ring), 0.12, and 0.10 nm was corresponding to the inner to outer rings. The ring assignments are shown in Fig. 5f.

Nanoparticles that are 3–4.5 nm in diameter were observed in another area of the same specimen of Ni-Im<sub>170</sub>, as shown in Fig. 6a (a bright-field image) and Fig. 6b (a dark-field image). Furthermore, the SAD pattern (Fig. 6c) showed a very weak ring with a *d*-value of 0.20 nm.

Drastic growth was observed on Ni-Im<sub>150</sub>, as shown in Fig. 7. A few nanoclusters with a diameter of 2 nm on the thin sheets were observed at the beginning of the TEM observation of this area, as shown in Fig. 7a (see Electronic Supplementary Material for an enlarged image of Fig. 7a). At this stage, the SAD analysis revealed a pattern similar to that of 2:1 trioctahedral phyllosilicates (Fig. 7b). After the first TEM observation, the nanoparticles grew drastically to 30 nm (diameter) in 10 min (Fig. 7c). The SAD pattern (Fig. 7d) taken after this drastic growth indicated the diffraction assigned to each plane of Ni, which confirmed that the grown nanoparticles were Ni nanoparticles. The diffraction spots were also seen overlapping with the diffraction rings, indicating the disordered crystal

orientations of each nanoparticle. Such a drastic growth was observed only in the case of Ni-Im<sub>150</sub>.

Figure 8 presents the changes of Ni-Im<sub>150</sub> under TEM with increasing illumination beam current. Initially, the SAD pattern (Fig. 8b) revealed broad diffraction rings attributed to the 2:1 phyllosilicate-like layer. Next, the TEM image (Fig. 8a) taken under a low illumination beam current of approximately 2 pA/cm<sup>2</sup> exhibited only a few nanoclusters smaller than 2 nm on the thin sheets at the beginning of the TEM observation of this area. A series of TEM images (Fig. 8c) examined under increasing illumination beam current (31–60 pA/cm<sup>2</sup>) indicated only slight growth. However, when the illumination beam current was increased to 120 pA/cm<sup>2</sup>, the nanoclusters grew drastically to sizes of 10–20 nm in diameter (Fig. 8d). Subsequently, the observed SAD pattern (Fig. 8e) exhibited the diffraction rings assigned to Ni.

At the beginning of the growth of the nanoclusters under TEM (e.g., as shown in Fig. 5a–c), the nanoclusters would incorporate Ni in the sub-nanoclusters (smaller than 1 nm) and/or the interlayer cation, Ni<sup>2+</sup>. There were three types of Ni species: nanoparticles (including nanoclusters and sub-nanoclusters), Ni<sup>2+</sup> within the interlayer space, and Ni<sup>2+</sup> in the octahedral sheet in the proposed models (Scheme 1 and/or 4 and chemical compositions 2 and/or 4). The interlayer cation (Ni<sup>2+</sup>) would compensate for the negative charge of the layer consisting of the phyllosilicate-like layer bonded

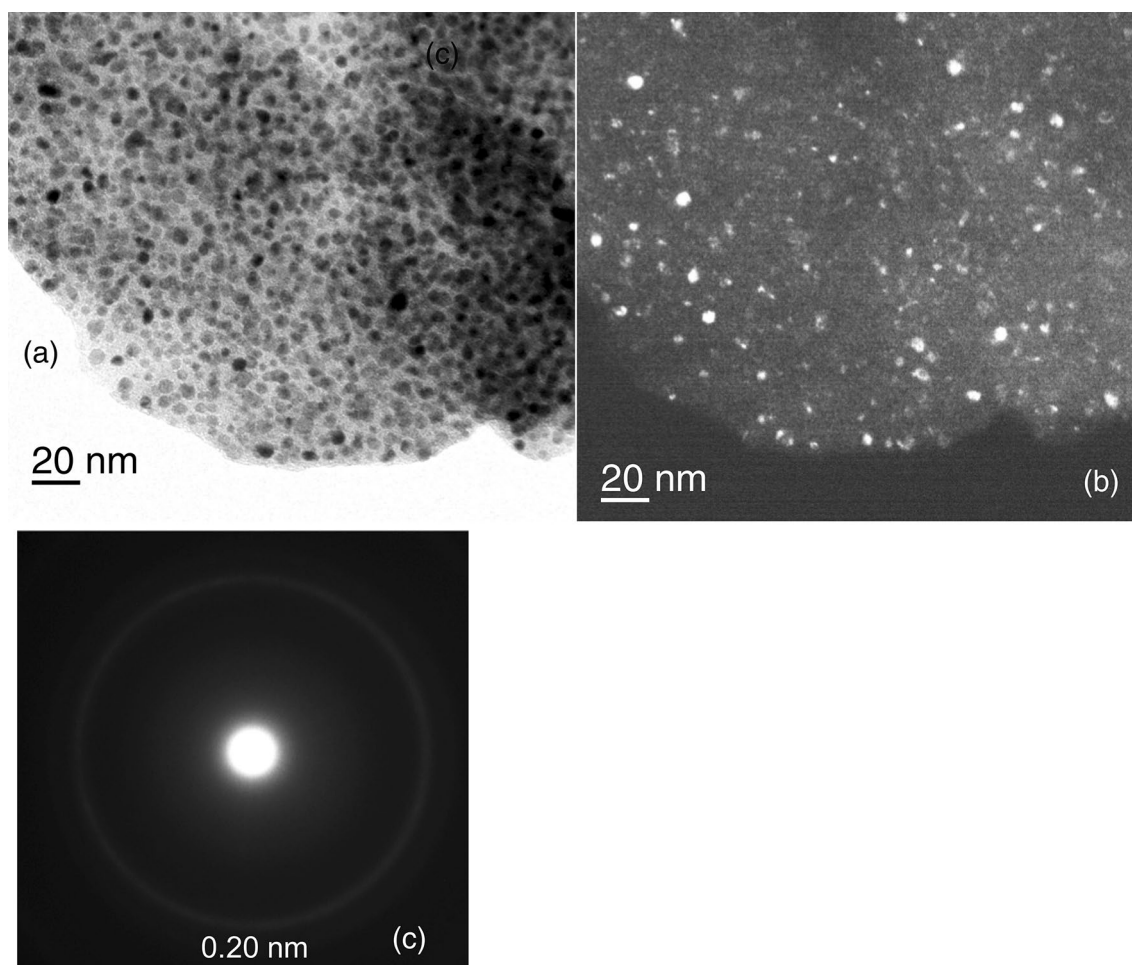


**Fig. 6** **a** Bright-field image, **b** dark-field image, and **c** SAD pattern for Ni-Im<sub>170</sub>

covalently with the imidazolyl group in a manner similar to 2:1 phyllosilicates. The SAD pattern showed the diffraction rings attributed to the 2:1 phyllosilicate-like layer after the beginning stage of the growth.

After further growth (Figs. 5c–e, 4a, b), the TEM images revealed that the thin sheets remained in the structure (Figs. 4b, 5e), in contrast to the SAD patterns, which did not exhibit any diffraction attributed to a structure similar to 2:1 phyllosilicates (Figs. 4c, 5f). This implies that the growing nanoclusters would take Ni<sup>2+</sup> from the cation octahedral sheet and the interlayer space for their growth. This withdrawal of a part of Ni<sup>2+</sup> from the cation octahedral sheet and/or the interlayer space would cause a broken structure

(the long-range periodic structure with ordered atomic arrangements) of the 2:1 phyllosilicate-like layer without disturbing the morphology of the thin sheets (Figs. 4b, 5e). Another interpretation of the results could be that the Ni in the nanoclusters and/or sub-nanoclusters would be reduced during the growth of Ni nanoparticles. The electrons could transfer from the phyllosilicate-like layer and/or imidazolyl group to the growing nanoclusters. The electrons could then reduce the growing particles. This reduction by the transferred electron could be the reason for the SAD patterns attributed to Ni after the growth. Simultaneously, the withdrawal of electrons could cause the decomposition of the phyllosilicate-like structure.

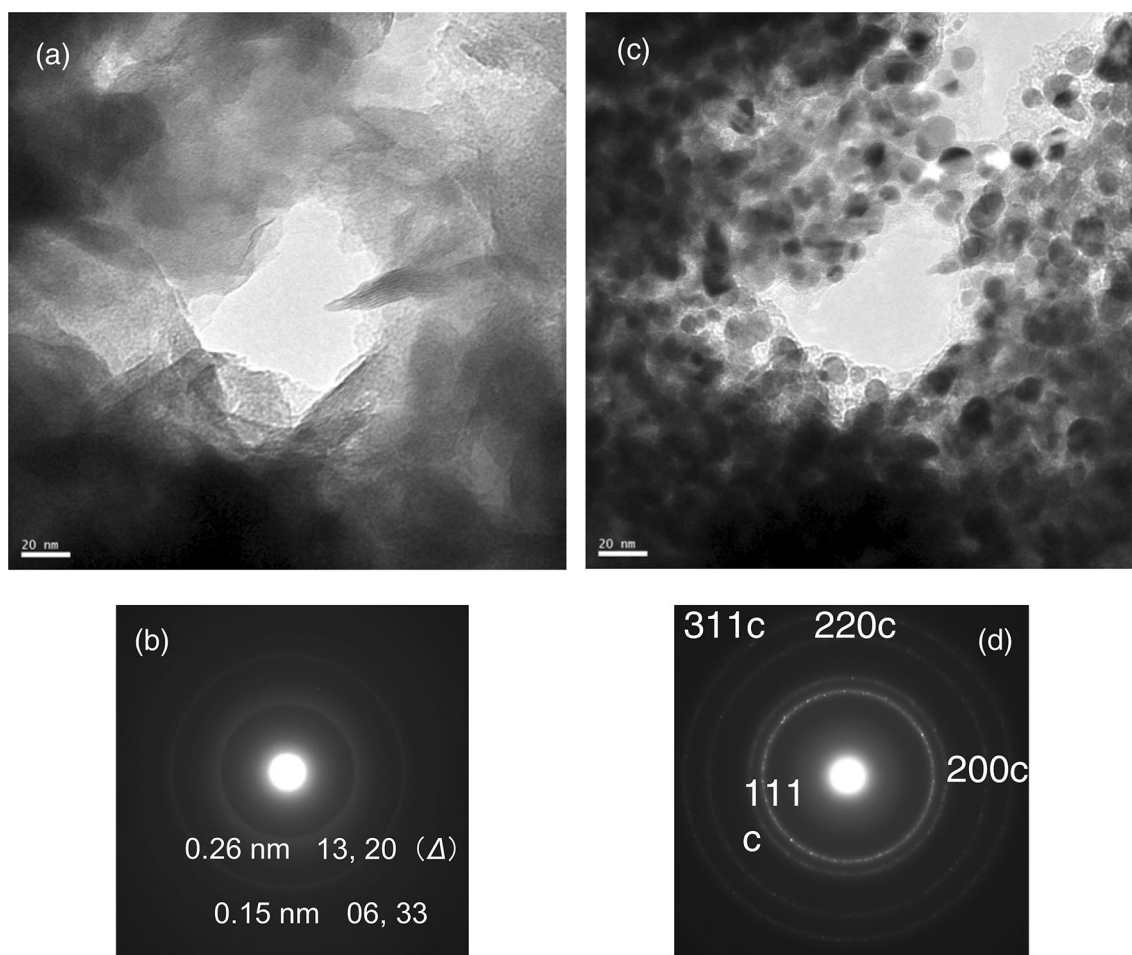


**Fig. 7** **a** and **c** TEM images and **b** and **d** SAD patterns for Ni-Im<sub>150</sub>

## 4 Conclusion

The TEM analyses revealed that nanoclusters with diameters of 1–2 nm were loaded on Ni-Im<sub>170</sub> and Ni-Im<sub>150</sub>. The results indicate the direct synthesis of layered inorganic-imidazole covalently bonded hybrids loaded with nanoclusters. For Ni-Im<sub>170</sub> and Ni-Im<sub>150</sub>, we observed that the nanoclusters grew to Ni nanoparticles of 3–5 nm in diameter under TEM. For Ni-Im<sub>150</sub>, the TEM observations revealed further drastic growth to larger Ni nanoparticles with a diameter of 30 nm under TEM. Nanoclusters and Ni nanoparticles with small sizes have the potential to exhibit high efficiencies as adsorbents, sensors, junction materials, conductive paste, internal electrodes, magnetic materials, and catalysts for

decomposing toxic organic compounds and for H<sub>2</sub> production. There is an imidazolyl group in addition to the nanoclusters present within the interlayer spaces of Ni-Im<sub>170</sub> and Ni-Im<sub>150</sub>. Therefore, the interlayer space can easily intercalate organic compounds and would allow the coexistence of toxic organic compounds and the nanoclusters. The catalysts can then act with high efficiency when they coexist with the targeted organic compounds within such a confined nanospace. This study reports, for the first time, the growth of nanoclusters and Ni nanoparticles under TEM and the direct synthesis of layered compounds loaded with nanoclusters. The results suggest the possibility of controlling the size of nanoclusters and Ni nanoparticles and fabricating patterned films, circuits, etc., by electron beam irradiation.

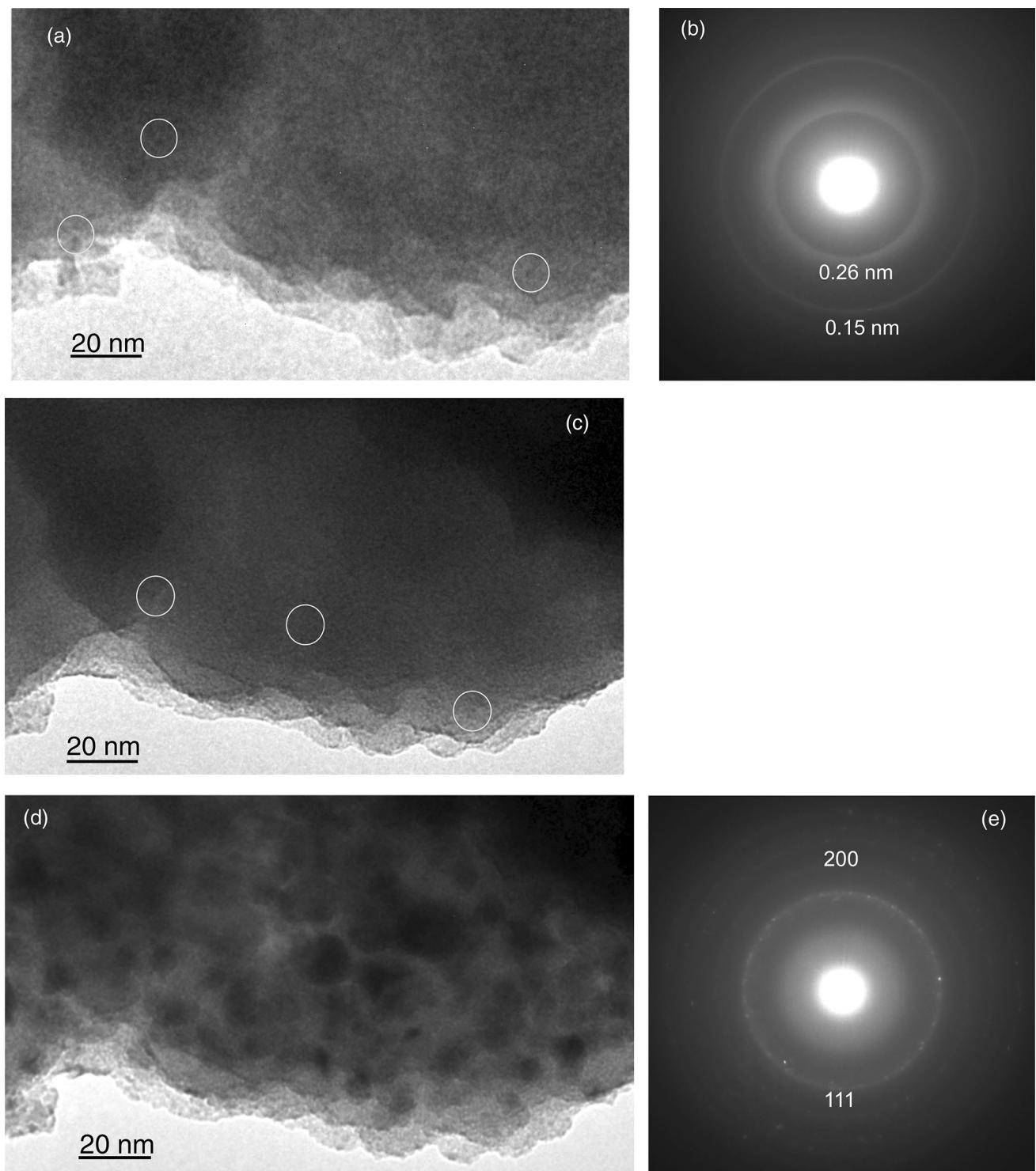


**Fig. 8** **a**, **c** and **d** TEM images and **b** and **e** SAD patterns for Ni-Im<sub>150</sub> with increasing beam current densities: **a** and **b** 2, **c** 60, and **d** and **e** 120 pA/cm<sup>2</sup>

**Acknowledgements** We are grateful to Mr. S. Takenouchi, NIMS, for the elemental analyses. This study was partially supported by Japan Society for the Promotion of Science (JSPS) KAKENHI (Grant Number 26420678).

## References

1. Y. Fukushima, M. Tani, *Bull. Chem. Soc. Jpn.* **69**, 3667 (1996)
2. Y. Fukushima, M. Tani, *J. Chem. Soc. Chem. Commun.* **1995**, 241 (1995)
3. K.A. Carrado, L. Xu, R. Csencsits, J.V. Muntean, *Chem. Mater.* **13**, 3766 (2001)
4. M. Guillot, M. Richard-Plouet, S. Vilminot, *J. Mater. Chem.* **12**, 851 (2002)
5. N.T. Whilton, S.L. Burkett, S. Mann, *J. Mater. Chem.* **8**, 1927 (1998)
6. M. Richard-Plouet, S. Vilminot, M. Guillot, *New J. Chem.* **28**, 1073 (2004)
7. K. Chabrol, M. Gressier, N. Pebere, M.J. Menu, F. Martin, J.P. Bonino, C. Marichal, J. Brendle, *J. Mater. Chem.* **20**, 9695 (2010)
8. M. Bruneau, J. Brendle, S. Bennici, L. Limousy, S. Pluchon, *New J. Chem.* **44**, 10326 (2020)
9. K. Fujii, S. Hayashi, H. Kodama, *Chem. Mater.* **15**, 1189 (2003)
10. K. Fujii, S. Hayashi, *Appl. Clay Sci.* **29**, 235 (2005)
11. K. Fujii, S. Hayashi, H. Hashizume, S. Shimomura, K. Jimura, T. Fujita, N. Iyi, A. Yamagishi, H. Sato, T. Ando, *Phys. Chem. Chem. Phys.* **18**, 19146 (2016)
12. K. Fujii, N. Iyi, R. Sasai, S. Hayashi, *Chem. Mater.* **20**, 2994 (2008)
13. K. Fujii, N. Iyi, H. Hashizume, S. Shimomura, T. Ando, *Chem. Mater.* **21**, 1179 (2009)
14. K. Fujii, T. Kuroda, K. Sakoda, N. Iyi, *J. Photochem. Photobiol. A* **225**, 125 (2011)
15. K. Fujii, J.P. Hill, H. Hashizume, S. Shimomura, K. Ariga, T. Ando, *J. Mater. Sci.* **52**, 12156 (2017)
16. L. Mercier, G.A. Facey, C. Detellier, *J. Chem. Soc. Chem. Commun.* **18**, 2111 (1994)
17. R. Ruiz-Hitzky, J.M. Rojo, *Nature* **287**, 28 (1980)
18. K. Fujii, H. Hashizume, S. Shimomura, T. Wakahara, T. Ando, *J. Inorg. Organomet. Polym. Mater.* **29**, 745 (2019)
19. K. Tanino, Y. Yokoyama, S. Fujiki, Y. Yamamichi, *J. Jpn. Inst. Electron. Package* **10**, 212 (2007)
20. R. Ueyama, T. Ueyama, K. Roumoto, K. Juribayashi, *J. Ceram. Soc. Jpn.* **108**, 769 (2000)
21. K. Nakano, *Chem. Lett.* **15**, 131 (2015)
22. H. Nishihara, F. Ohtake, A. Castro-Muniz, H. Itoi, M. Ito, Y. Hayasaka, J. Maruyama, J.N. Kondo, R. Osuga, T. Kyaotani, *J. Mater. Chem. A* **6**, 12523 (2018)
23. R.A. Ortega-Dominguez, H. Vargas-Villagrán, C. Penaloza-Orta, K. Saavedra-Rubio, X. Bokhimi, T.E. Klimova, *Fuel* **198**, 110 (2017)
24. J. Zhang, R. Tu, T. Goto, *J. Ceram. Soc. Jpn.* **121**, 226 (2013)
25. H. Sato, K. Kuramitsu, K. Sugawara, *J. Soc. Powder Technol. Jpn.* **41**, 645 (2004)
26. Z. Gui, R. Fan, W. Mo, X. Chen, L. Yang, Y. Hu, *Mater. Res. Bull.* **38**, 169 (2003)
27. H. Inokawa, M. Maeda, S. Nishimoto, Y. Kameshima, M. Miyake, T. Ichikawa, Y. Kojima, H. Miyaoka, *Int. J. Hydrogen Energy* **38**, 13579 (2013)
28. H. Inokawa, T. Ichikawa, H. Miyaoka, *Appl. Catal. A* **491**, 184 (2015)
29. Z. Hu, C. Weng, C. Chen, Z. Tuan, *Appl. Catal. A* **562**, 49 (2016)
30. I. Rossetti, M. Compagnoni, E. Finocchio, G. Ramis, A.D. Michele, A. Zucchini, S. Dzwigaj, *Int. J. Hydrogen Energy* **41**, 16878 (2016)
31. C. Lee, P. Lin, B. Chen, R.G. Kukushkin, V.A. Yakovlev, *Catal. Today* (2020). <https://doi.org/10.1016/j.cattod.2020.05.013>
32. L. Wang, R.T. Yang, *J. Phys. Chem. C* **112**, 12486 (2008)
33. L. Wei, Y. Mao, *Int. J. Hydrogen Energy* **41**, 11692 (2016)
34. J.L. Regalbutto Jr., *J. Catal.* **260**, 329 (2008)
35. S.E. Bozbag, L.C. Zhang, M. Aindow, C. Erkey, *J. Supercrit. Fluids* **66**, 265 (2012)
36. M. Miyagawa, A. Shibusawa, K. Maeda, A. Tashiro, T. Sugai, H. Tanaka, *RSC Adv.* **7**, 41896 (2017)
37. M. Miyagawa, Y. Ikeyama, H. Kotake, T. Maeda, H. Tanaka, *Chem. Phys. Lett.* **753**, 137615 (2020)
38. T. Fujimura, Y. Yoshida, H. Inoue, T. Shimada, S. Takagi, *Langmuir* **31**, 9142 (2015)
39. Q. Yuan, T.D. Golden, *Surf. Interfaces* **20**, 100620 (2020)
40. R.D. Shannon, *Acta Cryst.* **A32**, 751 (1976)
41. Nihonkagakukai, *Kagakubinran Kisoheon*, 4th edn. (Maruzen, Tokyo, 1993), pp. II-725
42. H.E. Swanson, E. Tatge, *Natl. Bur. Stand. (U. S.), Circ.* **539(1)**, 13 (1953)

**Publisher's Note** Springer Nature remains neutral with regard to jurisdictional claims in published maps and institutional affiliations.